Structure and Oxygen-Sensing Paramagnetic Properties of a New Lithium 1,8,15,22-Tetraphenoxyphthalocyanine Radical Probe for Biological Oximetry

Ramasamy P. Pandian,[†] Michelle Dolgos,[‡] Vinh Dang,[†] Joe Z. Sostaric,[†] Patrick M Woodward,[‡] and Periannan Kuppusamy*,[†]

Davis Heart and Lung Research Institute, Department of Internal Medicine and Department of Chemistry, The Ohio State University, Columbus, Ohio

Received March 5, 2007. Revised Manuscript Received April 13, 2007

The synthesis, physicochemical properties, X-ray powder structure, electrochemical, and oxygen-sensing properties of a new phenoxy-substituted lithium phthalocyanine (lithium 1,8,15,22-tetraphenoxyphthalocyanine, LiPc-α-OPh) radical probe are presented. LiPc-α-OPh was synthesized in the form of a microcrystalline powder by an elctrochemical method and characterized by UV−visible, IR, ^{1}H NMR, EPR, and mass spectroscopy. The UV−visible spectrum of LiPc-α-OPh showed a bathochromic shift of absorption bands due to delocalization of the π- electron density into the phenoxy ring. X-ray powder diffraction studies revealed a structural framework that possesses long, hollow channels running parallel to the packing direction. The channels measured approximately 4.9 × 8.7 Å^2 in the two-dimensional plane perpendicular to the length of the channel, allowing for diffusion of oxygen molecules (2.9 × 3.9 Å^2) through the channel. The powder exhibited a single, sharp EPR line under anoxic conditions, with a peak-to-peak line width of 530 mG. The line width was sensitive to surrounding molecular oxygen, showing a linear increase to pO_2 with an oxygen-sensitivity of 13.7 mG/mmHg. LiPc-α-OPh microcrystals can be further prepared as nanosized crystals for possible cellular internalization, but without losing its oxygen-sensing properties. Thus, the LiPc-α-OPh crystals could be useful as a reliable probe for biological oximetry.

Introduction

Metallophthalocyanines are a group of multifunctional materials that have been utilized in industry and biolgy in a variety of applications such as dyestuffs,[1−7] sensors,[8−10] liquid crystals,[11−13] and photodynamic therapy.[14−17] Notably, lithium phthalocyanine (LiPc) is a stable neutral radical exhibiting an intrinsic semiconducting behavior with unusual magnetic properties. LiPc has been synthesized and investigated in details.[18−31] However, synthesis of LiPc in a pure and

* Corresponding author. Address: 420 West 12th Avenue, Room 114, Ohio State University, Columbus, OH 43210. Fax: 614-292-8454. Tel: 614-292-8998. E-mail: kuppusamy.1@osu.edu.

‡ Department of Chemistry, The Ohio State University.

† Department of Internal Medicine, The Ohio State University.

(1) *Phthalocyanines: Properties and Applications*; Lenznoff, C. C., Lever, A. B. P., Eds.; VCH Publishers: Weinheim, Germany, 1996; Vol. 1−4.
(2) *The Porphyrin Handbook*; Kadish, K. M., Smith, K. M., Guilard, R., Eds.; Academic Press: San Diego, 2003; Vol. 15−20.
(3) de la Torre, G.; Claessens, C. G.; Torres, T. *J. Chem. Soc., Chem. Commun.* **2007**, DOI: 10.1039/b614234f.
(4) de la Torre, G.; Vazquez, P.; Agullo-Lopez, F.; Torres, T. *Chem. Rev.* **2004**, *104*, 3723−3750.
(5) Evenou, F.; Abdulkarim, E. M.; Pons, M. N.; Zahraa, O.; Benhammou, A.; Yaacoubi, A.; Nejmeddine, A. *Dyes Pigm.* **2007**, *74*, 439−445.
(6) McKeown, N. B. In *Phthalocyanine Materials: Synthesis, Structure and Function*; McKeown, N. B., Ed.; University Press: Cambridge, UK, 1998.
(7) Peng, X.; Draney, D. R.; Volcheck, W. M.; Bashford, G. R.; Lamb, D. T.; Grone, D. L.; Zhang, Y.; Johnson, C. M. *Proc. SPIE.−Int. Soc. Opt. Eng.* **2006**, 6097.
(8) Collins, R. A.; Mohammed, K. A. *J. Phys. D: Appl. Phys.* **1988**, *21*, 154−161.
(9) Guillaud, G.; Simon, J.; Germain, J. P. *Chem. Soc. Rev.* **1998**, *170−180*, 1433−1484.
(10) Pandian, R. P.; Dang, V.; Manoharan, P. T.; Zweier, J. L.; Kuppusamy, P. *J. Magn. Reson.* **2006**, *181*, 154−161.
(11) Clarkson, G. J.; McKeown, N. B.; Treacher, K. E. *J. Chem. Soc., Perkin Trans. I* **1995**, 1817−1823.
(12) Duro, J. A.; Gema, D. T.; Barbera, J.; Serrano, J. L.; Torres, T. *Chem. Mater.* **1996**, *8*, 1061−1066.
(13) McKeown, N. B. *Chem. Ind.* **1992**, 92.
(14) Bonnet, R. *Chem. Soc. Rev.* **1995**, *24*, 19.
(15) Brown, S. B.; Truscott, T. G. *Chem. Br.* **1993**, *29*, 955.
(16) Kalka, K.; Ahmad, N.; Criswell, T.; Boothman, D.; Mukhtar, H. *Cancer Res.* **2000**, *60*, 5984−5987.
(17) Phillips, D. *Pure. Appl. Chem.* **1995**, *67*, 117.
(18) Afeworki, M.; Miller, N. R.; Devasahayam, N.; Cook, J.; Mitchell, J. B.; Subramanian, S.; Krishna, M. C. *Free Radical Biol. Med.* **1998**, *25*, 72−78.
(19) Andre, J. J.; Brinkmann, M. *Synth. Met.* **1997**, *90*, 211−216.
(20) Bensebaa, F.; Andre, J. J. *J. Phys. Chem.* **1992**, *96*, 5739−5745.
(21) Bensebaa, F.; Petit, F.; Andre, J. J. *Synth. Met.* **1992**, *52*, 57−69.
(22) Brinkmann, M.; Andre, J. J. *J. Mater. Chem.* **1999**, *9*, 1511−1520.
(23) Brinkmann, M.; Turek, P.; Andre, J. J. *J. Mater. Chem.* **1998**, *8*, 675−685.
(24) Ilangovan, G.; L., Z. J.; Kuppusamy, P. *J. Magn. Reson.* **2004**, *170*, 42−48.
(25) Ilangovan, G.; Li, H.; Zweier, J. L.; Kuppusamy, P. *J. Phys. Chem. B* **2001**, *105*, 5323−5330.
(26) Ilangovan, G.; Manivannan, A.; Li, H.; Yanagi, H.; Zweier, J. L.; Kuppusamy, P. *Free Radical Biol. Med.* **2002**, *32*, 139−147.
(27) Ilangovan, G.; Pal, R.; Zweier, J. L.; Kuppusamy, P. *J. Phys. Chem. B* **2002**, *106*, 11929−11935.
(28) Ilangovan, G.; Zweier, J. L.; Kuppusamy, P. *J. Phys. Chem. B* **2000**, *104*, 9404−9410.
(29) Ilangovan, G.; Zweier, J. L.; Kuppusamy, P. *J. Phys. Chem. B* **2000**, *104*, 4047−4059.
(30) Liu, K. J.; Gast, P.; Moussavi, M.; Norby, S. W.; Vahidi, N.; Walczak, T.; Wu, M.; Swartz, H. M. *Proc. Natl. Acad. Sci. U.S.A.* **1993**, *90*, 5438−5442.
(31) Turek, P.; Andre, J. J.; Giraudeau, A.; Simon, J. *Chem. Phys. Lett.* **1987**, *134*, 471−475.

10.1021/cm070622k CCC: $37.00
Published on Web 06/14/2007

desirable oxygen-sensitive form has been a critical problem and a challenge in this field. LiPc exhibits three distinct crystalline polymorphs, namely the α, *β*, and x-forms, all of which are EPR active, but only the x-form is oxygen-sensitive.[18,23,24,28,29] Another distinct difficulty in the synthesis of LiPc lies in the ability to reproducibly control the composition and oxygen sensitivity of the material; different batches of the same preparations of LiPc tend to yield crystals with wide variations in the oximetry properties.

The electron paramagnetic resonance (EPR) properties of LiPc are of particular interest for several reasons. LiPc exhibits a single and narrow-line in the EPR spectrum, the width of which is highly sensitive to the concentration of the surrounding molecular oxygen.[22−24,28,29,31,32] The EPR line width is dependent on electron delocalization at the phthalocyanine moiety, the extent of packing of the molecules and the efficiency of the $\pi-\pi$ interaction between the molecules. The spin density in the LiPc molecule is higher on the inner ring, where alternating nitrogen and carbon atoms exist, the latter being highly implicated in the intermolecular overlap.[33] Any modification of the molecule, in particular substitution on the external rings by electron-donor or -acceptor groups, would be expected to have an effect on the line width and oxygen sensitivity of LiPc for a number of reasons. First, substitution on the external rings by such groups could modify the spin delocalization on the molecule. It will also invariably result in changes in the intermolecular interactions between adjacent molecules within the crystal. Furthermore, the substitution could hamper the free diffusion of electrons through channels that run through the crystalline structure of LiPc particulates.[22,23,29]

Such substitution reactions have been performed; for example, the substitution of the external protons of the ring structure by methoxy, an electron-donor group, resulted in the formation of a polycrystalline LiPc powder.[21] However, the alkoxy-substituted lithium phthalocyanines are unstable and easily demetalate to give a mixture of dilithium phthalocyanines and metal-free phthalocyanines.[34−36] Furthermore, as the length of the alkoxy chain in phthalocyanine increases, the stability of these lithium derivatives decreases.[34−36]

In continuation of our investigation of lithium phthalocyanine radicals as EPR oximetry probes for biological applications, we report on the synthesis, physicochemical, structural, and oxygen-sensing paramagnetic properties of a new radical, lithium 1,8,15,22-tetraphenoxyphthalocyanine (LiPc-α-OPh), containing a phenoxy-substitution at the α-position in the phthalocyanine ring (Figure 1). The radical is prepared as a microcrystalline solid by an electrochemical method. The material possesses distinct structural and paramagnetic properties that are favorable for oximetry applications. It has a high oxygen sensitivity and stability in tissues as compared to LiPc and is capable of providing accurate and reliable measurements of oxygen concentrations in biological systems.

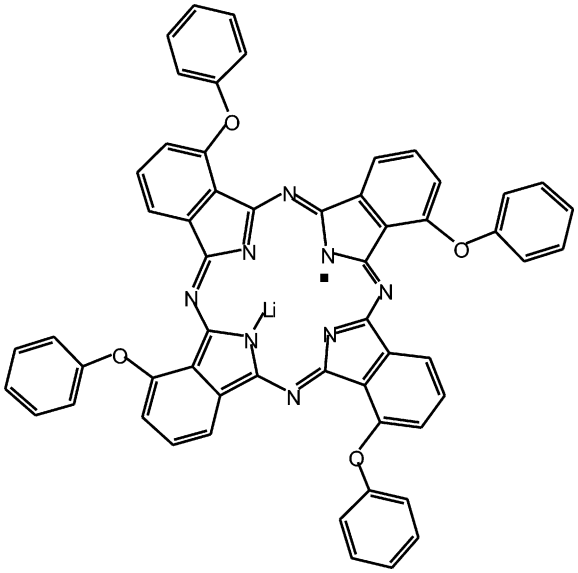

Figure 1. Molecular structure of the lithium 1,8,15,22-tetraphenoxyphthalocyanine (LiPc-α-OPh) radical.

Materials and Methods

Lithium granules, *n*-pentanol, tetrahydrofuran, acetontrile, and tetrabutylammonium perchlorate (TBAP) were obtained from Aldrich (St. Louis, MO). 3-Phenoxyphthalonitrile was synthesized using the procedure described by Derkacheva and Luk'yanets.[37]

Synthesis of Dilithium 1,8,15,22-Tetraphenoxyphthalocyanine (Li_2Pc-α-OPh). Lithium granules (150 mg) and 3-phenoxyphthalonitrile (1.35 g, 6.12 mmol) were added to *n*-pentanol (20 mL) and refluxed for 8 h under an atmosphere of dry nitrogen. After being cooled to room temperature, the solvent was evaporated under reduced pressure and the dry residue was dissolved in 300 mL of acetonitrile and filtered. The blue-green solution was slowly evaporated until a dry residue remained. The residue, which is dilithium 1,8,15,22-tetraphenoxyphthalocyanine (Li_2Pc-α-OPh), was washed with cold acetontrile (10 mL) and then dried under a vacuum. The yield was 0.53 g, 39%. Microanalysis of the product was in good agreement with the formula of Li_2Pc-α-OPh. Found: C, 73.99; H, 3.99; N, 12.04; Li, 1.57. Calcd for $C_{56}H_{32}N_8O_4Li$: C, 75.17; H, 3.6; N, 12.52; Li, 1.55. NMR: δ 7.0−7.6 ppm (m).

Synthesis of Lithium 1,8,15,22-Tetraphenoxyphthalocyanine (LiPc-α-OPh) Radical. For bulk electrochemical synthesis of LiPc-α-OPh, a bigger platinum mesh electrode with a very high surface area (BAS, West Lafayette, IN) was used as the working electrode in a large-volume electrolysis cell. The electrochemical cell setup and electrolysis were carried out according to the reported procedure.[18,29] Briefly, 150 mL of acetonitrile containing 0.1 M TBAP was added to 200 mg of Li_2Pc-α-OPh with constant stirring so that all Li_2Pc-α-OPh added was completely dissolved. The resultant blue-green solution was transferred to one of the two compartments of the cell. A potential of +0.7 V was used to prepare the LiPc-α-OPh. Because the resulting LiPc-α-OPh is insoluble in acetonitrile, the electrolysis product was either precipitated out at the bottom of the cell or stuck to the electrode surface with poor adherence. During electrolysis, the solution was continuously purged with argon to remove dissolved oxygen. The bulk electrolysis was

(32) Turek, P.; Petit, P.; Andre, J. J.; Simon, J.; Even, R.; Boudjema, B.; Guillaud, G.; Maitrot, M. *J. Am. Chem. Soc.* **1987**, *109*, 5119−5122.
(33) Gotschy, B.; Denninger, G. *Mol. Phys.* **1990**, *71*, 169.
(34) Deng, X.; Porter, W.; Vaid, T. P. *Polyhedron* **2005**, *24*, 3004−3011.
(35) Pandian, R. P.; Kuppusamy, P. **2007**, unpublished results,
(36) Petit, M. A.; Thami, T.; Sirlin, C.; Lelievre, D. *New J. Chem.* **1991**, *15*, 71−74.
(37) Derkacheva, V. M.; Luk'yanets, E. A. *Zh. Obsh. Khim.* **1980**, *50*, 2313−2318.

Scheme 1

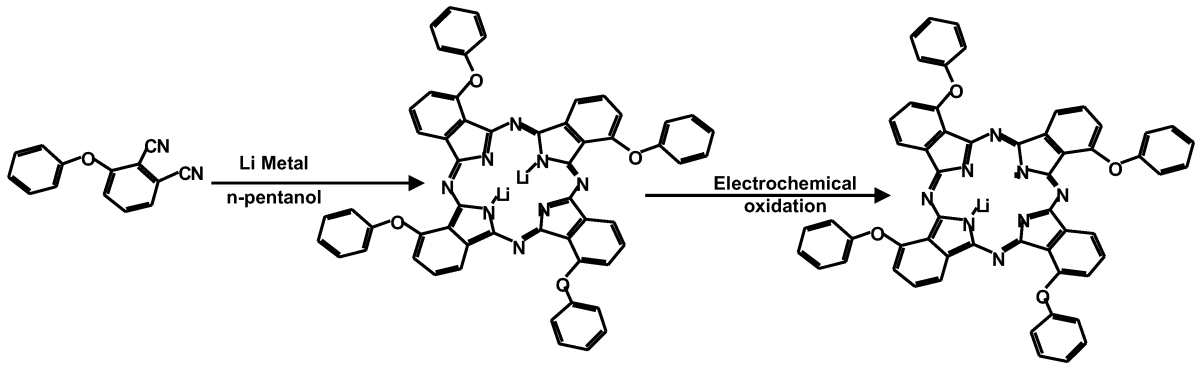

carried out to ensure that by the end of the electrolysis the current remained constant at the level of the background current. After electrolysis, the small fraction of LiPc-α-OPh sticking to the electrode surface, as well as the bulk, was filtered and dried at 90 °C under atmospheric conditions to obtain a shiny dark-green powder. Microanalysis of the product was in good agreement with the formula of LiPc-α-OPh. Found: C, 75.03; H, 4.06; N, 12.29; Li, 0.88. Calcd for $C_{56}H_{32}N_8O_4Li$: C, 75.17; H, 3.6; N, 12.52; Li, 0.78. MS-LCT electrospray: exact mass *m*/*z* calcd for $C_{56}H_{32}N_8O_4$-Li (M^+), 887.2707; found, 887.2706.

Preparation of LiPc-α-OPh Nanoparticulates. Microcrystalline particulates of LiPc-α-OPh were suspended in phosphate buffered solution (PBS) (10 mg/0.5 mL) and sonicated a total of 5 times at 30 s intervals, with a microtip titanium horn and a generator power setting of 5. The particulate suspension was cooled for 1 min between each successive 30 s burst of sonication. At the end of sonication, the suspension was placed in ice for 2 min to allow the heavier particulates to settle down at the bottom of the tube, and the supernatant possessing smaller-sized particles was transferred to a separate tube. Particle-size analysis was conducted with a Zetasizer (Malvern Instruments, model nano-s) with the capability of characterizing particle sizes ranging from 0.6 nm to 10 μm. The supernatant contained fine particulates of LiPc-α-OPh with a particulate size of <300 nm.

EPR Measurements. EPR measurements were carried out at 9.78 GHz (X-band) using a Bruker model ER300 EPR spectrometer (Billerica, MA). Data acquisition and analysis were performed using a personal computer (PC) interfaced to the spectrometer. Instrument control, data acquisition, and data processing were performed using software developed in the laboratory. Unless mentioned otherwise, the EPR linewidths reported in this manuscript were peak-to-peak width (ΔBpp) of the first derivative spectra.

Calibration of LiPc-α-OPh for EPR Oximetry. EPR line width versus pO_2 calibration curves were constructed from X-band EPR measurements. The calibration measurements were performed as follows. A small amount (~10 μg) of the LiPc-α-OPh powder was encapsulated in a 0.8 mm diameter gas-permeable Teflon tube (Zeus Industrial Products, Orangeburg, SC) and the tube was sealed at both ends. The sealed sample was inserted into a 3 mm open quartz EPR tube. Desired compositions of oxygen and nitrogen gas mixtures were obtained by mixing different ratios of purified oxygen and nitrogen gases. A precalibrated gas-flow meter (Cole-Parmer, Vernon Hills, IL) with two separate inlets was used to mix the gases in any desired ratio, and the mixture was sent through gas-impermeable silicon tubes into the EPR tube. The EPR tube was placed in the TM_{110} microwave cavity (X-band) in such a way that the sample was at the center of the active volume of the resonator. All measurements were carried out after equilibrating the sample with the gas mixture for at least 10 min. The flow rate of the gas mixture was maintained at 2 dm^3/min. The total pressure inside the EPR tube was maintained at 760 mmHg, because the other end of the EPR tube was open to the atmosphere.

Optical Absorption Measurements. UV−visible−near IR absorption spectra were measured using a Cary 50 spectrophotometer in the wavelength range of 200−1100 nm. Infrared (IR) spectra were recorded by a Perkin-Elmer SpectrumOne FTIR spectrophotometer (Wellesley, MA).

Electrochemical Measurements. All the electrochemical measurements were carried out in dry acetonitrile (Aldrich, HPLC grade) using a CHI electrochemical analyzer controlled by a personal computer. The conventional three-electrode setup was used. In the chronoamperometric and cyclic voltammetric (CV) studies, platinum (Pt), Ag/AgCl, and Pt foil were used as the working, reference, and auxiliary electrode, respectively. The TBAP was used as the supporting electrolyte.

X-ray Powder Diffraction Measurements. X-ray powder diffraction was performed using a Bruker D8 diffractomer. The instrument uses a Cu−Kα radiation tube (λ = 1.5406 Å) together with an incident beam Ge monochromator and a Braun linear position sensitive detector. The patterns were collected in capillary mode at room temperature. The sample was packed in a 1 mm diameter glass capillary and data was collected over a 2θ range from 3 to 40° using a step size of 0.014347° and a counting time of 15 s per step.

Results and Discussion

The dilithium salt of tetraphenoxy-substituted phthalocyanine (Li_2Pc-α-OPh) was synthesized by cyclotetramerization of 3-phenoxyphthalonitrile in the presence of lithium pentoxide, as shown in Scheme 1. Elemental analysis, IR, and UV−visible spectroscopic data of Li_2Pc-α-OPh were in accordance with the proposed structure. In the ^{1}H NMR spectrum of Li_2Pc-α-OPh, the aromatic protons appeared at δ 7.0−7.68 ppm. The absence of the 3285 cm^{-1} band corresponding to the NH stretching absorption in the IR spectrum indicated the absence of the metal-free form of the tetraphenoxyphthalocyanine (Pc-α-OPh).

Cyclic voltametric studies were carried out on Li_2Pc-α-OPh to obtain the optimum conditions for its oxidation to LiPc-α-OPh radical. Figure 2 shows the cyclic voltammogram (CV) of Li_2Pc-α-OPh in dry acetonitrile at a potential sweep rate of 50 mV s^{-1}. The full CV pattern encompassing the potential range −0.25 to +1.0 V shows two processes. The first and second oxidations occur at +0.31 and +0.833 V and were irreversible. In the first process, the cathodic peak was not observed in equal magnitude as the counterpart at +0.056 V in the reverse sweep. The second oxidation

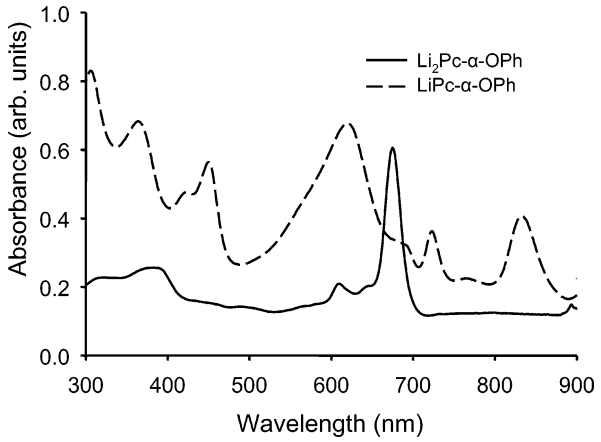

Figure 2. UV−visible−near IR spectra of Li_2Pc-α-OPh and LiPc-α-OPh in THF.

process is an irreversible oxidation that occurs beyond +0.751 V and there is no cathodic counterpart. The Li_2Pc-α-OPh has a higher oxidation potential in comparison to Li_2-Pc[18,29,31] because of the resonance interaction between the Pc moiety and the phenoxy ring; there is a reduction in the π-electron density in the Pc moiety, resulting an increase in the oxidation potential.

Electrolysis of Li_2Pc-α-OPh in acetonitrile at 0.7 V (vs Ag/AgCl electrode) gave the LiPc-α-OPh radical in the form of a microcrystalline powder. The powder was characterized by optical, X-ray, and EPR spectroscopic techniques.

Optical Properties of LiPc-α-OPh in Solution. The electronic absorption spectra of Li_2Pc-α-OPh and LiPc-α-OPh in THF are shown in Figure 2. The spectrum of LiPc-α-OPh showed Q bands at 833, 722, and 619 (br.) nm and Soret bands at 449 (split), 421, and 364 nm. The Li_2Pc-α-OPh showed a strong Q-band at 674, 610, and 381 (br.) nm. The absorption bands of LiPc-α-OPh were bathochromically shifted relative to the Li_2Pc-α-OPh. The split in the Q-band for LiPc-α-OPh was due to the fact that its symmetry was lowered relative to Li_2Pc-α-OPh. The explanation for this observation is that the phenoxy groups are electron-withdrawing, making the phenoxy-subsituted phthalocyanine less basic than unsubstituted phthalocyanines. The addition of phenoxy groups facilitates electron delocalization of the π-electrons into the phenoxy ring by a resonance interaction; such a resonance interaction is supported by the UV−visible spectra (Figure 2). The UV−visible spectrum of LiPc-α-OPh exhibited a bathochromic shift into the near-infrared region indicating that the resonance interaction between the phthalocyanine moiety and phenoxy is stronger in LiPc-α-OPh in comparison to LiPc. The increased solubility of Li_2-Pc-α-OPh in organic solvents in comparison to Li_2Pc can be attributed to a reduction of the intermolecular interactions between phthalocyanine rings, possibly due to the phenoxy substitution.[38]

Optical and Confocal Microscopy of LiPc-α-OPh Crystals. The microcrystalline powder of LiPc-α-OPh was analyzed using optical microscopy (Figure 4A) to confirm that the resultant powder was predominantly crystalline in

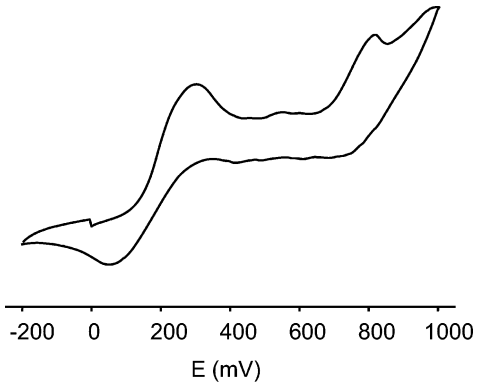

Figure 3. Cyclic voltammogram of Li2Pc-α-OPh in dry acetonitrile containing 0.2 M of TBAP measured at 25 °C. A Pt wire was used as the working electrode. The scan rate was 50 mV/s. Potentials are displayed relative to the Ag/AgCl electrode.

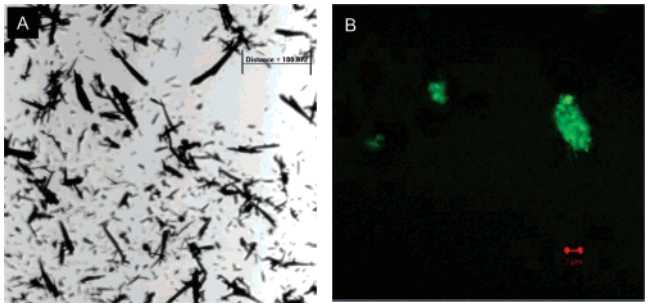

Figure 4. Optical images of LiPc-α-OPh microcrystals. (A) Microscopic image at 20× magnification. (B) Confocal microscopic image using an excitation wavelength of 488 nm showing a weak green fluorescence.

nature. The confocal fluorescence microscopic studies of LiPc-α-OPh crystals excited at 488 nm gave a weak green fluorescence image (Figure 4B), indicating that LiPc-α-OPh particulates can be dectected by confocal microscopy.

X-ray Crystal Structure of LiPc-α-OPh. The molecular packing of microcrystalline LiPc-α-OPh was determined using real space structure solution methods to extract structural information from X-ray powder diffraction data. The first step in the process is to determine the unit-cell parameters. This was done using the autoindexing software suite of Topas Academic.[39] Twenty-five peaks were present in the diffraction pattern. Their positions were determinined by profile fitting and used as input for the autoindexing algorithm. Several plausible triclinic cells were found; however, the best solutions had similar cell volumes, strongly suggesting they were equivalent solutions. To test the validity of the preferred solution, we carried out whole pattern fitting, using the Pawley Method[40] as implemented in Topas. The best Pawley fit gave unit-cell parameters of $a = 5.6188(11)$ Å, $b = 15.2756(13)$ Å, $c = 13.9060(18)$ Å, $\alpha = 77.886(2)°$, $\beta = 109.019(1)°$, and $\gamma = 91.803(2)°$. The unit-cell volume (1102.387 Å^3) yields a very reasonable value of 1.337 g/cm^3 for the density, if we assume one molecule per unit cell ($Z = 1$). Unreasonable densities are obtained for alternate choices of Z.

After determining the unit-cell dimensions, the DASH software package was used to determine the molecular packing of LiPc-α-OPh.[41,42] Peak intensities were extracted

(38) Ma, C.; Tian, D.; Hou, X.; Chang, Y.; Cong, F.; Yu, H.; Du, X.; Du, G. *Synthesis* **2005**, 741−748.

(39) Coelho, A. A. *Topas-Academic* **2004**,

(40) Pawley, G. S. *J. Appl. Crystallogr.* **1981**, *14*, 357−361.

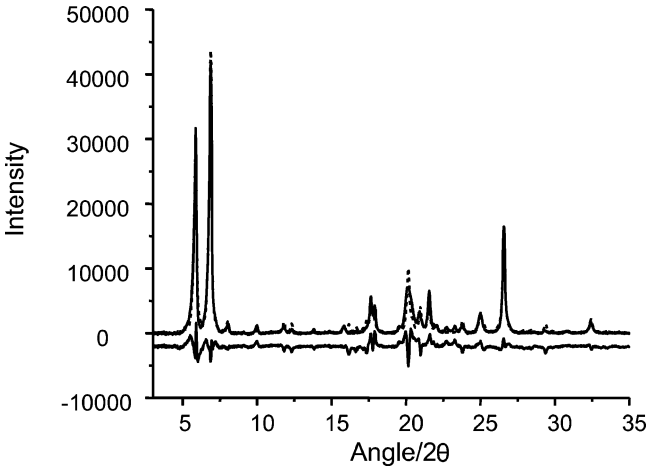

Figure 5. X-ray powder diffraction pattern of LiPc-α-OPh. The observed pattern is shown as a solid line, whereas the calculated pattern from the simulated annealing procedure is shown with a dashed line. The difference pattern is plotted underneath.

in DASH via a whole pattern-fitting algorithm based on the Pawley method. The Pawley fit yielded a χ^2 value of 7.029 and an R_{wp} value of 0.0943.

The molecular geometry was created using the Materials Studio software package.[43] For triclinic symmetry there are only two choices of space group, $P\bar{1}$ and $P1$. Our initial assmption was to assume that LiPc-α-OPh adopts the more commonly encountered $P\bar{1}$ symmetry. Having already determined that there is only one molecule per unit cell, the presence of an inversion center means that only one-half of the molecule is crystallographically unique. This also constrains the position of the center of the molecule to lie on the inversion center. Because of the rigidity of the phthalocyanine ring, only seven variables were needed to describe the crystal structure of LiPc-α-OPh; three variables to describe rotational degrees of freedom and four variables to account for the torsion angles of the phenoxy rings.

Forty simulated annealing runs were performed in which each individual run consisted of 20 million moves (5500 moves at each temperature) to determine the best fit to the experimental data. Of these 40 runs, the χ^2(pro) values ranged from 59.3 to 68.5. Reproducibility of the packing and the orientation of the phenoxy rings were consistent among the solutions.

Upon further examination, the intensities of the $(1\bar{1}1)$, and the $(1\bar{1}2)$ peaks were underestimated in the calculated pattern. Inspection of the structure revealed that the phthalocyanine rings lay horizontally along the $1\bar{1}2$ plane. Taken together, these two observations raise the possibility of preferred orientation, which most likely originates from the needle-like habit of the crystals (see Figure 4A). Consequently, the simulated annealing runs were performed again, under the same conditions, while taking preferred orientation along the $1\bar{1}2$ plane into account. This improved the fit significantly, as shown in Figure 5, giving χ^2(pro) values ranging from 39.48 to 45.40. Despite the improvement in the fit, inspection of the structure showed that introduction of the preferred orientation correction caused relatively little change in the molecular packing.

A simulated annealing run was also performed with the space group $P1$. When using $P1$ symmetry, the entire molecule becomes crystallographically unique and the location of the molecule is no longer constrained by symmetry. This increases the number of variables from 7 to 10. Despite the increased number of variables, the quality of the fit was not improved from the $P\bar{1}$ result. Therefore, the higher-symmetry $P\bar{1}$ space group can be taken to be correct. In addition, simulated annealing runs were performed under the same conditions on three other possible unit cells obtained from the autoindexing process, but all of them resulted in χ^2(pro) values greater than 100. As a result, these solutions were discarded.

Finally a rigid body Rietveld refinement was performed on the solution with the lowest χ^2(pro) value using the DASH suite. Only the global isotropic temperature factor, torsion angles and rotation variables were refined. The preferred orientation along the $(1\bar{1}2)$ plane was also taken into account. Overall this improved the quality of fit, χ^2(pro), from 39.48 to 32.37. A refinement of the bond angles and bond distances was attempted, but although this improved the quality of the fit, the refined parameters were unrealistic and greatly distorted the shape of the phenoxy rings as well as the phthalocyanine ring.[26,27] Clearly, there is not a sufficient number of diffraction peaks to warrant the rigid bond constraints of the planar region of the molecule. For riged body structure solution using DASH, a solution is generally considered to be acceptable if the χ^2(pro) value after the Rietveld refinement stage is within a factor of ~5 from the χ^2 value obtained in the Pawley refinement. In this case, χ^2(pro)/ χ^2(Pawley) is ~4.6 (32.37/7.03).

Figure 6 shows the torsions of the phenoxy groups in LiPc-α-OPh. As shown in Figure 7, the molecules are arranged in a slip-stacked columns held together by $\pi-\pi$ stacking of the phthalocyanine rings, similar to that seen in potassium phthalocyanine (KPc) as well as the α and β forms of LiPc.[23,29,44] The distance between the LiPc planes is approximately 3.36 Å, and the slipping distance is 4.65 Å. The distance between phthalocyanine planes is very similar in LiPc (3.245 Å) and LiPc-α-OPh (3.36 Å). So we see that although the phenoxy rings increase the spacing between molecules in neighboring chains, the intrachain molecular separations in LiPc-α-OPh are not greatly perturbed by the phenoxy substituents. The neighboring columns of molecules are held together along the *c*-axis by the $\pi-\pi$ stacking of the phenoxy rings as can be seen in Figure 8.

The packing of the LiPc-α-OPh molecules creates possible open channels that allow for the movement of oxygen molecules, whose size is approximately 2.8×3.9 Å^2. Running parallel to the *a*-axis, there are two types of open channels. The first type of channel (labeled 1 in Figure 8) lies between phenoxy rings from two adjacent molecules that

(41) David, W. I. F.; Shankland, K.; Shankland, N. *Chem. Commun.* **1998**, 931−932.
(42) David, W. I. F.; Shankland, K.; van de Streek, J.; Pidcock, E.; Motherwell, W. D. S.; Cole, J. C. *J. Appl. Crystallogr.* **2006**, *39*, 910−915.
(43) *Materials Studio*; Accelrys: San Diego, CA, 2001.
(44) Margadonna, S.; Prassides, K.; Iwasa, Y.; Taguchi, Y.; Craciun, M. F.; Rogge, S.; Morpurgo, A. F. *Inorg. Chem.* **2006**, *45*, 10472−10478.

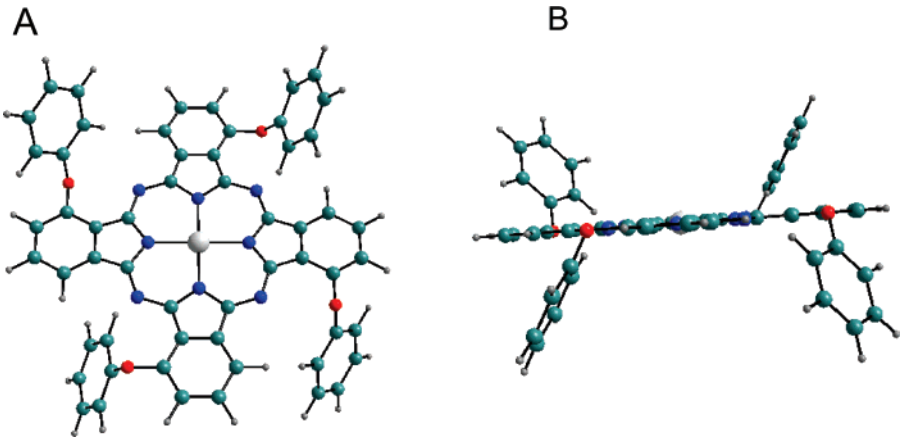

Figure 6. Molecular structure of LiPc-α-OPh (A) viewed perpendicular to the (1−1 2) plane, and (B) along the plane of the phthalocyanine ring.

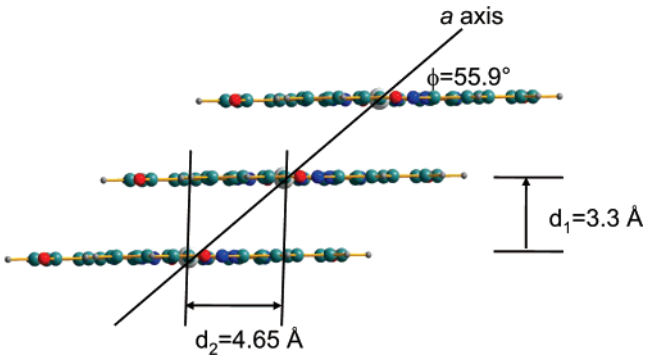

Figure 7. Slip-stacked pattern of LiPc-α-OPh along the crystallographic *a*-axis. The phenoxy rings were removed from the figure for clarity.

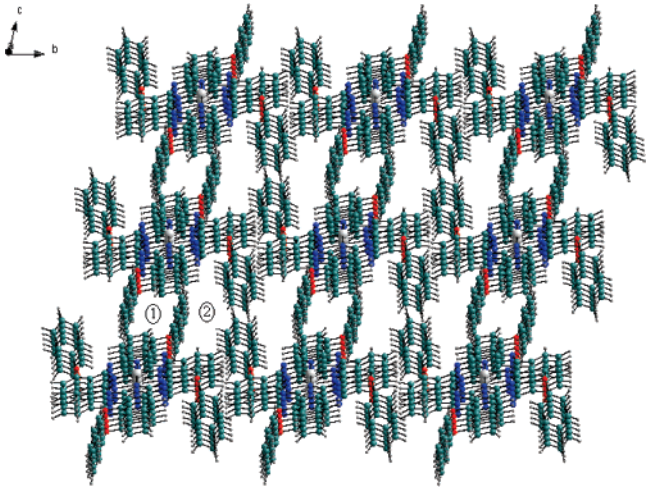

Figure 8. Stacking pattern of LiPc-α-OPh showing a large channel between the molecules. The two channels are labeled (1) between the phenoxy rings of neighboring LiPc-α-OPh molecules and (2) a longer, narrow channel between the molecules.

lie parallel but in a staggered orientation to one another. The size of this channel is approximately 4.9 × 4.6 Å^2. It is not clear if these channels are sufficiently large to allow for diffusion of O_2 molecules, particularly given the $\pi-\pi$ stacking interactions of the phenoxy rings. However, another channel can be found running parallel to the *a*-axis (labeled 2 in Figure 8). Its dimensions are defined by four adjacent LiPc-α-OPh molecules. This space is considerably larger than the area between the phenoxy rings of neighboring molecules and forms an oval-shaped channel with dimensions of approximately 4.6 × 8.7 Å^2. Figure 9 shows a 3D space-filled representation of the stacked molecules, which displays the two channels described above.

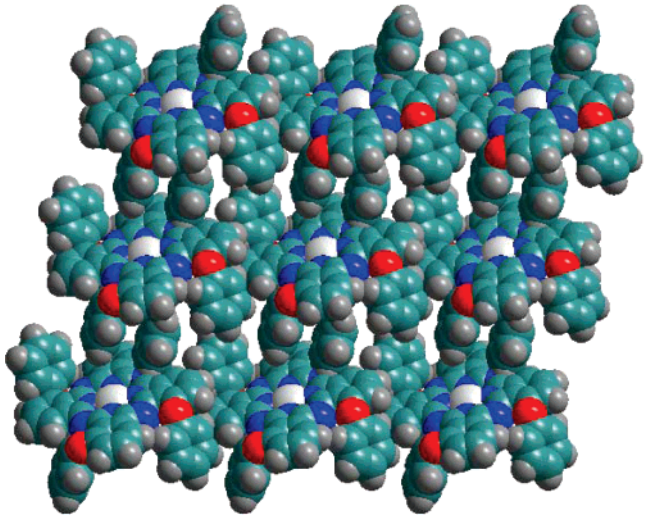

Figure 9. Space-filling model of stacked LiPc-α-OPh with the same view as in Figure 7, looking down the *a*-axis showing the possible channels for oxygen transport.

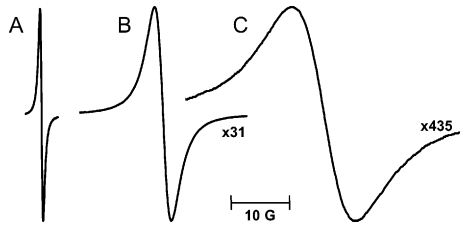

Figure 10. EPR spectra of LiPc-α-OPh. The spectra of LiPc-α-OPh powder obtained under vacuum (A), in the presence of 20.9% O_2/80% N_2 (B), and 100% O_2 (C) are shown at indicated magnification. The EPR instrumental settings were microwave frequency, 9.78 GHz; microwave power, 0.5 mW; modulation amplitude, 150 mG; modulation frequency, 100 kHz; receiver time constant, 41 ms; acquisition time, 15 s (single scan). A single peak is observed with a peak-to-peak width of 0.530, 2.930, and 11.030 G, corresponding to vacuum, 20.9% O_2, and 100% O_2, respectively.

EPR Studies of LiPc and LiPc-α-OPh. The X-band EPR spectrum of LiPc-α-OPh microcrystals, measured under a vacuum, consists of a single sharp peak with a peak-to-peak width of 0.530 G (Figure 10). The observation of a single line ensures that there is only one paramagnetic form of LiPc-α-OPh present in the particulate sample. The observed line width of LiPc-α-OPh is significantly larger than the reported values for LiPc crystals (0.01−0.05 G).[19,23−25,27−30,45] The

line width LiPc-α-OPh was highly sensitive to the surrounding amount of molecular oxygen. For example, the linewidths under room air (20.9% oxygen) and in the presence of 100% oxygen at atmospheric pressure were 2.930 and 11.030 G, respectively (Figure 10). Line shape analysis of the powder spectra showed that the shape was predominantly Lorentzian (data not shown). This indicated that the anisotrophy of the *g*-factor and line width were small or undectable within the limit of experimental resolution.

The observation of a single sharp line in the EPR spectrum of lithium phthalocyanine radical crystals is a common feature that is attributed to the phenomenon of exchange narrowing.[19,23,29] The x-form of LiPc, a structurally related analog of LiPc-α-OPh without the phenoxy substitution, contains a tetragonal unit cell with straight molecular packing along the *c*-axis and with an interplanar LiPc−LiPc spacing of 3.245 Å.[46] The straight columnar packing leads to channels of approximately 6 Å in diameter along the stack axis. The rather short interplanar distance and large interstack separation result in one-dimensional spin diffusion along the stack axis.[19,23,29] LiPc-α-OPh presents a markedly different molecular packing pattern from that of LiPc because of the steric and electronic effects of the phenoxy groups and macrocyclic π-ligands. The X-ray analysis of LiPc-α-OPh revealed that the gap between the LiPc-α-OPh planes is ∼3.36 Å in comparison to LiPc, which has an interplanar distance of 3.245 Å.[19,23,29,46,47] The slipping distance in LiPc-α-OPh is relatively larger attributed to a substantial steric interaction by the phenoxy groups in LiPc-α-OPh, which is absent in the case of LiPc. The subtle increase in stacking distance and/or the inductive effect caused by the phenoxy group in LiPc-α-OPh are responsible for a wider line width and weaker spin exchange properties, as seen in the EPR measurements. The steric phenoxy group in LiPc-α-OPh may withdraw a substantial amount of the π-electron density from the phthalocyanine moiety, leading to significant retardation of spin diffusion along *a*-axis. These effects may account for the larger anoxic line width in LiPc-α-OPh (0.53 G) in comparison to LiPc (0.01−0.05 G).[19,23−25,27−30,45] It should be noted that the anoxic width of lithium octamethoxyphthalocyanine (LiPc-OMe)[21] is not very different from that of LiPc, suggesting that the spin-exchange interactions in both cases may not be different. However, the crystalline packing in LiPc-OMe is not known.

A notable problem with the synthesis of LiPc-α-OPh is the failure to grow crystals of an adequate size for single-crystal X-ray analysis. It has been reported that both unsubstituted phthalocyanines and phthalocyanines with small substituents[21] show highly ordered growth, whereas phthalocyanines with larger substituents tend to show a disordered growth.[48] The different degree of order is attributed to different molecule−molecule interactions. The ordered growth is enhanced by strong interactions between π systems of the molecules.[48−50] Thus, the free rotation of phenoxy rings and large intermolecular separations in LiPc-α-OPh may lead to less-ordered growth of LiPc-α-OPh crystals.

Effect of Molecular Oxygen on the EPR Spectrum of LiPc-α-OPh. The presence of molecular oxygen broadens the EPR spectrum of the LiPc-α-OPh as shown in Figure 10. The broadening of the EPR spectrum in the presence of molecular oxygen is due to the Heisenberg intermolecular spin exchange between the LiPc-α-OPh probe and molecular oxygen and subsequent shortening of the spin−spin relaxation time.[51] The variation of the peak-to-peak width of the EPR line with pO_2 observed for LiPc-α-OPh is shown in Figure 11A. The line width increased linearly with pO_2 over the entire 0 to 760 mmHg range, indicating that the spin-exchange increases linearly with pO_2. An important observation is that the slope of the line width versus pO_2 calibration line, which reflects the sensitivity of the probe to pO_2, is large (13.7 mG/mmHg). The effect of oxygen on the EPR line width or intensity was reversible on cycles of oxygenation-deoxygenation processes (data not shown). A similar oxygen-induced broadening of the EPR spectrum has been observed for LiPc, lithium naphthalocyanines, and chars.[24−30,52−58] Unlike many soluble EPR probes that show a linear dependence of their line width with concentration of oxygen. It is well-known that the calibration curves of many particulate probes have a tendency to depart from linear behavior at higher pO_2. This behavior has a number of origins, including saturation of the oxygen interaction with spin states of the probe,[24,28,29,59] adsorption of oxygen in the micropores of the probe,[60] or severe limitation of the transport of gas-phase paramagnetic species into microchannels penetrating the structure.[61] The linear variation of line width with pO_2 observed for LiPc-α-OPh up to 760 mmHg suggests that oxygen is transported freely into its channel, without any adverse chemical or physical interactions. The relatively larger channel bore-size in LiPc-α-OPh may explain the higher oxygen sensitivity in LiPc-α-OPh (13.7 mG/mmHg)

(45) Turek, P.; Andre, J. J.; Simon, J. *Solid State Commun.* **1987**, *63*, 741−744.
(46) Sugimoto, H.; Mori, M.; Masuda, H.; Taga, T. *J. Chem. Soc., Chem Commun.* **1986**, 962−963.
(47) Sugimoto, H.; Higashi, T.; Mori, M. *J. Chem. Soc., Chem. Commun.* **1983**, 622−623.
(48) Hassan, B. M.; Li, H.; McKeown, N. B. *J. Mater. Chem.* **2000**, *10*, 39−45.
(49) Peisert, H.; Biswas, I.; Zhang, L.; Knupfer, M.; Hanack, M.; Dini, D.; Cook, M. J.; Chambrier, I.; Schmidt, T.; Batchelor, D.; Chassé, T. *Chem. Phys. Lett.* **2005**, *406*, 1−6.
(50) Peisert, H.; Schwieger, T.; Auerhammer, J. M.; Knupfer, M.; Golden, M. S.; Fink, J.; Bressler, P. R.; Mast, M. *J. Appl. Phys.* **2001**, *90*, 466−469.
(51) Hyde, J. S.; Subczynski, W. K. In *Biological Magnetic Resonance*; Plenum Press: New York, 1988; Vol. 18, p 399.
(52) Gallez, B.; Jordan, B. F.; Baudelet, C. *Magn. Reson. Med.* **1999**, *42*, 193−196.
(53) Goda, F.; Liu, K. J.; Walczak, T.; O'Hara, J. A.; Jiang, J.; Swartz, H. M. *Magn. Reson. Med.* **1995**, *33*, 237−245.
(54) Liu, K. J.; Miyake, M.; James, P. E.; Swartz, H. M. *J. Magn. Reson.* **1998**, *133*, 291−298.
(55) Manivannan, A.; Yanagi, H. *Chem. Lett.* **2001**, 568−569.
(56) Manivannan, A.; Yanagi, H.; Ilangovan, G.; Kuppusamy, P. *J. Magn. Magn. Mater.* **2001**, *233*, L131−L135.
(57) Pandian, R. P.; Kim, Y.; Woodward, P. M.; Zweier, J. M.; Manoharan, P. T.; Kuppusamy, P. *J. Mater. Chem.* **2006**, *16*, 3609−3618.
(58) Pandian, R. P.; Parinandi, N. L.; Ilangovan, G.; Zweier, J. L.; Kuppusamy, P. *Free Radical Biol. Med.* **2003**, *35*, 1138−1148.
(59) Atsarkin, V. A.; Demidov, V. V.; Vasneva, G. A.; Dzheparov, F. S.; Ceroke, P. J.; Odintsov, B. M.; Clarkson, R. B. *J. Magn. Reson.* **2001**, *149*, 85−89.
(60) Kanemoto, K.; Yamauchi, J. *J. Phys. Chem. B* **2001**, *105*, 2117−2121.
(61) Zhdanov, V. *Adv. Colloid Interface Sci.* **1996**, *66*, 1−21.

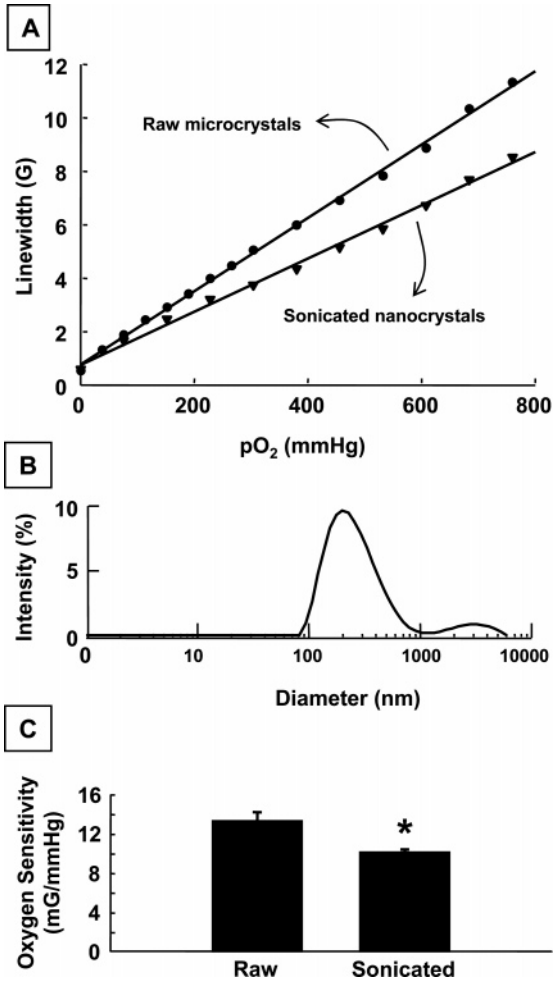

Figure 11. Effect of molecular oxygen on the EPR line width of LiPc-α-OPh crystals. (A) Variation of line width with pO_2 for raw (micro) and sonicated (submicro/nano) crystals from a single batch. A linear variation of line width with the pO_2 is observed. The probe sensitivity (as measured by the slope) is 13.7 mG/mmHg for microcrystals and 9.7 mG/mmHg for sonicated nanocrystals. (B) Size-distribution profile of particles obtained by sonicating a suspension containing 5 mg/mL raw LiPc-α-OPh microcrystals. (C) Effect of sonolysis on the oxygen sensitivity of LiPc-α-OPh crystals. Values are expressed as mean ± SD from 4 independent batches of LiPc-α-OPh preparation; *significantly ($p < 0.05$) different from raw crystals.

as compared to that in LiPc (5−9 mG/mmHg)[20,23−25,27−29] crystals.

Effect of Crystal Size on the Oxygen Sensitivity of LiPc-α-OPh.

A consequence of possible disordered growth of LiPc-α-OPh crystals is the difficulty in the reproducibility of crystal size and oxygen calibration from batch to batch. Our preparations showed variations of 20−50 mG in anoxic line width and oxygen sensitivity as well. To obtain particles of uniform size/sensitivity, we generally reduce the size of particles from the raw preparations by sonication. The particle-size distribution for LiPc-α-OPh particles sonicated at 22.5 kHz showed that the particle suspension had a distribution with a maximum number of particles at approximately 180 nm and a size ranging from 100 to 300 nm. (Figure 11B). The sonicated particles retained both oxygen sensitivity and linearity in the line width versus pO_2 curve (Figure 11C). Regardless of the preparation batch, the sonicated particles always showed less variabilty in their oximetry calibration following sonolysis (Figure 11A). The results of sonolysis of LiPc-α-OPh is similar to that of sonolysis of LiPc crystals when exposed to ultrasound of a frequency of 20 kHz. However, it should be noted that exposure of LiPc microparticles to a combination of 20 kHz sonolysis, followed by higher frequency sonolysis (i.e., 354 kHz) was shown to result in a further decrease in particle size, but a striking loss of oxygen sensitivity.[62] The ability to form LiPc-α-OPh nanoparticles that remain sensitive to the partial pressure of oxygen is particularly advantageous for internalizing these nanoparticulates in cells for a variety of novel biological applications, including intracellular oximetry, cell-tracking, and oxygen measurements in stem cell therapy.

Conclusions

A new phenoxy-substituted, phthalocyanine-based radical probe, LiPc-α-OPh, was synthesized as fine crystals and characterized. The X-ray powder diffraction analysis showed that packing of LiPc-α-OPh molecules create open channels with size greater than 4.6×8.7 Å^2, which permits diffusion of oxygen molecules (2.8×3.9 Å^2) through the crystals. The probe showed an exchange-narrowed single line EPR spectrum that was sensitive to the surrounding oxygen concentration. The effect of molecular oxygen on the EPR line width was linear for up to 760 mmHg. LiPc-α-OPh nanopraticulates showed similar oxygen-sensitivity in a distinct comparison to LiPc nanoparticulates, which do not show oxygen-sensitivity. These results demonstrate that LiPc-α-OPh can be useful as an effective probe molecule for a variety of biological oximetry applications.

Acknowledgment. We acknowledge the financial support from the NIH grant EB 004031.

Supporting Information Available: Crystallographic information in CIF format. This material is available free of charge via the Internet at http://pubs.acs.org.

CM070622K

(62) Sostaric, J. Z.; Pandian, R. P.; Weavers, L. K.; Kuppusamy, P. *Chem. Mater.* **2006**, *18*, 4183−4189.